DOI 10.1007/s11595-017-1645-3

Mechanistic Studies of Atmospheric Corrosion Behavior of Al and Al-based Alloys in a Tropical Marine Environment

CUI Zhongyu[1], GE Feng[1], LI Xiaogang[2*], ZHU Min[3], XIAO Kui[2], DONG Chaofang[2], WANG Xin[1]

(1. Institute of Materials Science and Engineering, Ocean University of China, Qingdao 266100, China; 2. Corrosion and Protection Center, University of Science and Technology Beijing, Beijing 100083, China; 3. Lab of Multi-phase Deposition and Erosion, Zhejiang Sci-Tech University, Hangzhou 310018, China)

Abstract: Atmospheric corrosion behavior of pure Al 1050A, 5A02 and 6A02 aluminum alloys exposed to a tropical marine environment for 4 years was investigated. Synergetic effect of Cl^- deposition rate and time of wetness resulted in an abnormal increase in weight loss and a significant fluctuation in corrosion rate. Pitting corrosion occurred on the three metals. Pits on 5A02 alloy were easy to initiate and inclined to propagate laterally to form higher corrosion area and shallower corrosion pits, while pits on 6A02 alloy presented the opposite appearances. This was further confirmed by the cyclic polarization experiments.

Key words: aluminum; atmospheric corrosion; pitting corrosion

1 Introduction

Aluminum and its alloys have been widely used in the shipbuilding industry because of the increasing demands for lowering the weight of different ships due to the increase of their sizes or generally increasing the payload[1-3]. In those fields, aluminum alloys are usually exposed in outdoor marine atmospheres and they can be affected by different forms of corrosion such as pitting corrosion, intergranular corrosion or exfoliation corrosion, which may bring serious damage to the ships.

In general, the corrosive chloride ions and the high humidity are responsible for the corrosion attacks on aluminum in tropical marine atmosphere. As the chloride-containing particles deposit on the specimen surface, chloride ions are adsorbed on the Al-oxide film and break this layer. For pure Al, breakdown of the surface oxide may occur via one (or a combination) of the following mechanisms: (i) penetration of the oxide by chloride ions, (ii) thinning of the oxide by chloride ions or (iii) through flaws in the oxide at the nanoscopic level[4-7]. In respect to aluminum alloys, microgalvanic elements form due to the presence of intermetallic (IM) particles which will promote the localized corrosion[7,8]. There have been many published works about the pitting corrosion of various kinds of aluminum alloys in NaCl solution in laboratory[7-11], while the same topic concerned on field exposure test is rather scare[12,13]. Therefore, understanding of the pitting corrosion of aluminum alloys in natural atmospheric environments is necessary for the practical application of aluminum alloys.

In this work, the atmospheric corrosion behavior of Al-Mg series aluminum alloy 5A02 and the Al-Mg-Si series alloy 6A02, which are widely used for ship building[14,15], in contrast with pure Al 1050A was investigated. The corrosion rate was determined by the weight loss method and the effect of environmental conditions on the corrosion kinetics was analyzed. The pitting corrosion behavior of the three metals was discussed based on the filed exposure results and the laboratory cyclic polarization experiments.

2 Experimental

2.1 Materials preparation

Chemical compositions of the aluminum alloys

(Received: Oct. 14, 2016; Accepted: Jan. 26, 2017)

CUI Zhongyu (崔中雨): Ph D; E-mail: cuizhongyu@ouc.edu.cn

* Corresponding author: LI Xiaogang (李晓刚): Prof.; E-mail: lixiaogang@ustb.edu.cn

Funded by the Natural Science Foundation of Shandong Province (Nos.ZR2016EMB12, ZR2013DL007), China Postdoctoral Science Foundation (No. 2015M582139), National Natural Science Foundation of China (No. 41406106) and the Major State Basic Research Development Program of China (973 Program), (No.2014CB643300)

are listed in Table 1. Samples with the dimension of 100 mm × 50 mm × 2.5 mm were used for field exposure tests. Prior to the tests, all the specimens were ground down to 800 grit and then degreased by acetone followed by cleaning in ethanol. All the specimens were weighed (w_0) and the surface area (S) was measured before exposure. Then all the specimens were installed on a test rack with a inclination angle of 45° horizontal to the sky and facing south in Xisha Islands (112°20′E, 16°50′N), 100 meters from the coastline. The test duration was 4 years. Four replicate metal samples were retrieved from the exposure site after 1, 3, 6, 9, 12, 24 and 48 months. Three replicas were employed to determine the weight loss of the specimens, and the other one was used to analyze the corrosion morphology and corrosion products.

Table 1 Chemical compositions of pure Al 1050A, 5A02 and 6A02 aluminum alloys

Alloy	Chemical composition/wt%						
	Fe	Si	Cu	Mn	Zn	Mg	Al
1050A	0.23	0.13	0.01	-	-	-	bal.
5A02	0.25	0.5	0.03	0.4	-	2.4	bal.
6A02	0.5	0.9-1.2	0.26	0.2	0.2	0.5	bal.

2.2 Environmental conditions of the exposure site

Table 2 lists the environmental parameters and atmospheric pollutants measured at Xisha Islands during the exposure[16], as well as the atmosphere classifications based on ISO 9223[17]. The average temperature in Xisha marine atmosphere was 27 ℃ with the maximum temperature increasing up to 33.3 ℃ and the minimum temperature reducing to 20.1 ℃ which was also a relatively high temperature. The extreme relative humidity (RH) values oscillated between 61% and 94% with a mean value of 77%. Time of wetness (TOW), which is defined as the period during which a metallic surface was covered by adsorptive and/or liquid film of electrolyte, is another important factor that affects the corrosion behavior of metals in atmosphere. Schindelholz *et al*[18] summarized that the TOW determination methods represented in literature and practice could be categorized by the way in which TOW was treated – either as an environmental parameter or as a surface parameter. However, both kinds of methods including ISO 9223 and other indirect electrode sensors had their limitations[19-21]. In this work, the TOW was treated as an environmental parameter and was calculated according to ISO 9223[17], which defines TOW as the time during which the RH of the ambient environment is greater than 80% at temperature above 0 ℃. With this method, the approximate TOW in Xisha islands was 2562 h/year which belonged to the classification of τ_4[17]. As for the corrosive species precipitated on the samples, the Cl^- and SO_2 deposition rates were considered and measured using the method given by ISO 9225[22]. The Cl^- deposition rate was determined by the wet candle method and the SO_2 deposition rate was determined using alkaline surfaces of porous filter plates saturated by a solution of sodium carbonate. According to the results, the annual average deposition rate of chloride was 112.68 mg/m^2·d, which was classified to the S_2[17]. Meanwhile, the precipitation of SO_2 was less than 0.1 mg/m^2·d and the rain had a near-neutral pH of 6.5 because no heavy industry existed at the exposure site.

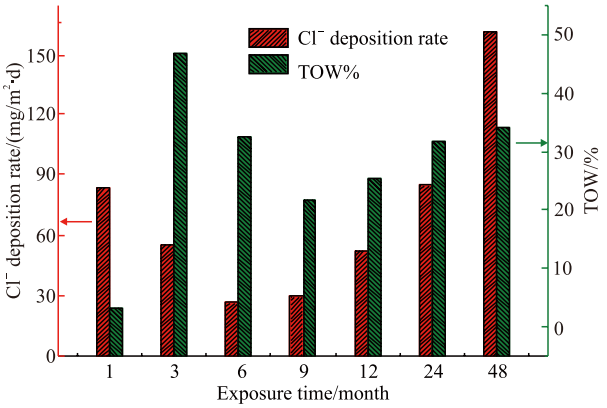

Fig.1 Variations of Cl^- deposition rate and time of wetness (TOW) during the exposure test

Variation of chloride ion deposition rate and TOW% as a function of exposure time is given in Fig.1, in which TOW% means the ratio of TOW to the total time during one exposure period. It was worthwhile

Table 2 Climatic parameters and atmospheric pollutants of Xisha Islands during 4 years exposure

Exposure site	Location	Max. temperature/℃	Min. temperature/℃	Average temperature/℃	Max. RH/%	Min. RH/%	Average RH/%
Xisha	112°20′E, 16°50′N	33.3	20.1	27	94	61	77
TOW/(h/year)	Rain/(mm/year)	Cl^- deposition rate /(mg/m^2·d)	SO_2 deposition rate /(mg/m^2·d)	Sunshine /(h/year)	pH of rain	Distance to sea/m	
2 562 (τ_4)	1 526	112.68 (S_2)	<0.1 (P_0)	2 675	6.5	100	

to note that the last three exposure periods, that was the exposure time from 12 months to 48 months, had a relatively higher Cl^- deposition rate and TOW, which influenced the weigh loss and corrosion rate of aluminum alloys.

2.3 Weight loss measurement

Corrosion products of the withdrawn triplicate specimens were chemically removed by pickling in the solution (50 mL H_3PO_4 + 20 g CrO_3 + 1 L H_2O) for 10 min at 80-100 ℃. After that, the specimens were rinsed with distilled water, dried in warm air and then weighed to obtain their final weights (w_1). The weight loss was calculated as follows:

$$C = \frac{w_0 - w_1}{S} \tag{1}$$

where C was the weight loss of the metal due to corrosion (g/m^2), w_0 was the original weight (g), w_1 was the final weight (g) and S was the surface area (m^2). The average corrosion rate of aluminum after exposure for different periods was calculated by using the equation in Ref.[23, 24]:

$$V_n = \frac{12(w_n - w_{n-1})}{t_n - t_{n-1}} \tag{2}$$

where V_n was the corrosion rate (g/m^2·year), w_n was the weight loss (g/m^2), t was the exposure time (month), n was the period of exposure (n=1, 2, 3, 4, 5, 6 and 7 referred to the sample exposed for 1, 3, 6, 9, 12, 24 and 48 months, respectively).

2.4 Characterization of corrosion morphologies

The corrosion morphologies of the exposed samples without corrosion products were observed by a scanning electron microscope (SEM, Quanta 250). The corrosion morphology without corrosion products taken by an optical microscope was processed by a binarization method to calculate the percentage of the corrosion coverage area.

2.5 Electrochemical measurements

Cyclic polarization curves were recorded in laboratory in 0.1 M NaCl solution to evaluate the pitting resistance of the three aluminum alloys. For all experiments a three-electrode cell was used, with a standard calomel electrode (SCE) being used as a reference electrode and a platinum counter electrode. All experiments were carried out on a CS350 electrochemical workstation at a constant room temperature of approximately 20 ℃. Cyclic polarizations were conducted by using an delay time at the equilibrium state of 60 min in order to stabilize the surface at open circuit potential (OCP). A polarization scan was carried out in the anodic direction, starting at 300 mV/SCE more negative than OCP, at a scan rate of 1 mV/s. The sweep direction was reversed at a limited threshold of 0.5 mA/cm^2. From the cyclic polarization curve, pitting potential (E_{pit}) and protection potential (E_{prot}) were obtained. To get reasonable values of these two parameters, the measurements were repeated more than ten times for a stochastic analysis.

3 Results

3.1 Weight loss and corrosion rate

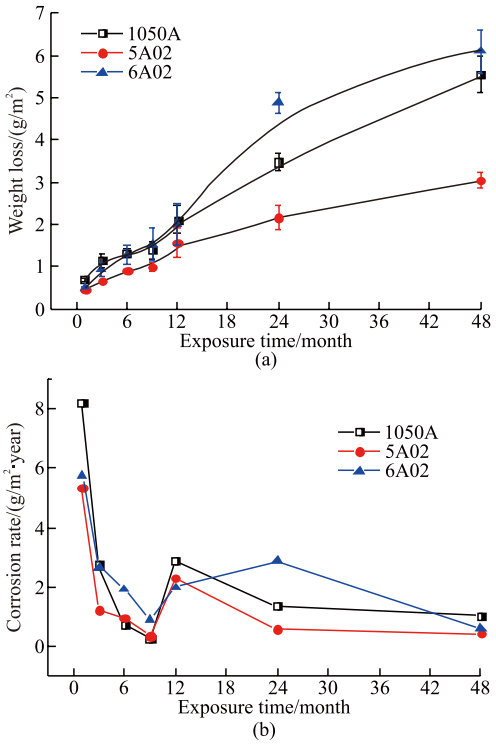

Fig.2 Weight loss (a) and corrosion rate (b) of pure Al 1050A, 5A02 and 6A02 aluminum alloys during exposure in Xisha marine atmosphere for 4 years

Fig.2 shows the weight loss (a) and the corrosion rate (b) of pure Al and its alloys during the 4-year exposure in Xisha marine atmosphere. An increasing trend in weight loss consisting of two different segments is observed in Fig.2(a). The weight loss of the three metals increases slowly during the initial 9 months of exposure, followed by a little faster augment until the end of the test. During the whole exposure periods, the weight loss of 5A02 alloy is lower than the other two metals. In the initial 12 months, the weight loss of 1050A and 6A02 is similar to each other.

However, it increases faster for the 6A02 alloy than the 1050A from 12 month to 48 month, resulting in the highest weight loss value of the 6A02 alloy. For the three metals, corrosion rates are the highest in the first month, followed by a significant decrease and achieve the lowest value after exposure for 9 months. From 9 to 48 months, a slight augment followed by a decline in corrosion rate is observed. The fluctuation of corrosion rate in Fig.2(b) is in accordance with the results of Ma who revealed that the corrosion rates in marine environment manifested a so-called "Reverse Phenomenon" in which the average corrosion velocity firstly augmented, and then decreased, and again suddenly increased in a certain period[25]. This special behavior only occurs in marine environment because of the effect of chloride[26]. Classification of corrosivity based on corrosion rate measurement of standard specimens according to ISO 9223 has been used to assess the atmospheric corrosion of aluminum in some literatures[27-29]. In Xisha islands, the corrosion rate of 1050A, 5A02 and 6A02 after exposure for 1 year is 2.12, 1.57 and 2.01 g/m^2·year, which belongs to the classification of C4, C3 and C4, respectively.

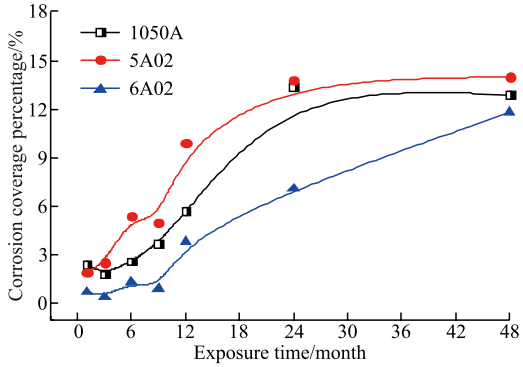

Fig.3 Corrosion coverage of pure Al 1050A, 5A02 and 6A02 aluminum alloys during the exposure test

3.2 Corrosion coverage

To investigate the corrosion propagation of aluminum and its alloys in the marine atmosphere, corrosion coverage, which represents the percentage of the corrosion area, is calculated and shown in Fig.3. It can be seen that corrosion coverage percentage exhibits a similar trend with the weight loss as the exposure time extends, both of which take the ninth month as the turning point. It is worthwhile to notice that the 5A02 alloy exhibits a higher corrosion coverage value than the 1050A pure Al, while that of the 6A02 alloy is lower than that of the 1050A during the whole exposure periods.

3.3 Corrosion morphology

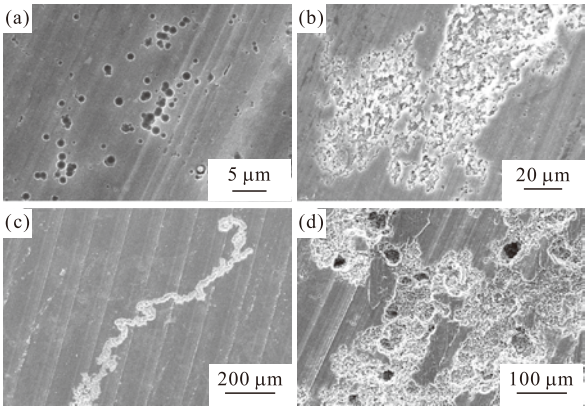

Fig.4 Corrosion morphologies of pure Al 1050A without corrosion products after exposure for (a) 1 month, (b) 6 months, (c) 12 months and (d) 48 months

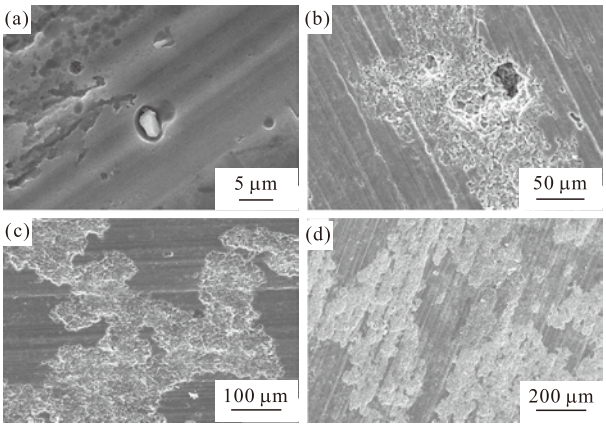

Fig.5 Corrosion morphologies of 5A02 aluminum alloy without corrosion products after exposure for (a) 1 month, (b) 6 months, (c) 12 months and (d) 48 months

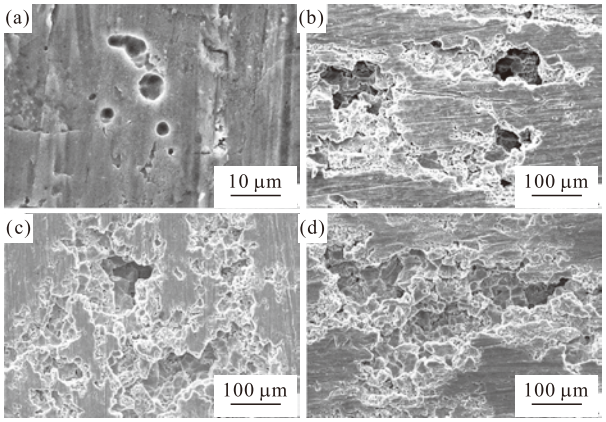

Fig.6 Corrosion morphologies of 6A02 aluminum alloy without corrosion products after exposure for (a) 1 month, (b) 6 months, (c) 12 months and (d) 48 months

Typical corrosion morphologies of 1050A after removing corrosion products are shown in Fig.4. A large number of shallow pits with a diameter less than 5 μm are found on the alloy surface after exposure for 1 month (Fig.4(a)). Besides them, there are also some stable pits formed on other area (not shown).

With the increase of the exposure time, some neighbor pits connect with each other and form a fringelike morphology as shown in Fig.4(b). By further increasing the exposure time, a noteworthy feature, which likes the filiform corrosion, is observed (Fig.4(c)). This is mainly attributed to the fluid electrolyte driven by gravity on the specimen surface. After 48 months, severe corrosion with large area corroded, accompanied by some isolated deep pits (Fig.4(d)).

Fig.5 shows the representative morphologies of 5A02 aluminum alloy during different stages of the exposure tests. Pits around intermetallic precipitates, which are identified as Al(Fe, Mn) particles by EDS, are observed on the sample exposed for 1 month. As the exposure extends, corrosion expands to the adjacent area and covers a larger region (Fig.5(b)). With further increasing of the exposure time, serious corrosion damage occurred on the alloy as shown in Figs.4(c) and d, in which the surface oxides are peeled off like a disbonded coating. It is worthy to note that no deep pits like that in 1050 A (Fig.4(d)) are detected.

Fig.6 shows the typical corrosion morphologies of 6A02 aluminum alloy during the exposure tests. After exposure for only 1 month, pits which are bigger than those formed on 1050A in Fig.4(a) are formed (Fig.6(a)). As the exposure time increases, the pits spread laterally and form deep holes on the specimen surface (Fig.6(b)). Further increasing the exposure time, those deep holes spread and connect to each other to form the ultimate morphology in Fig.6(d).

3.4 Cyclic polarization scans

In this section, pitting resistance of the aluminum and its alloys is evaluated by cyclic polarization (CP) curves. Fig.7 shows the CP curves of 1050A, 5A02 and 6A02 in aerated 0.1 M NaCl solution. It can be seen that the anodic part of the CP curves of 1050A and 6A02 aluminum alloy exhibits a distinct passive region, while the 5A02 alloy presents an active dissolution behavior. For 1050A and 6A02, the potential after which the anodic current has a sharp increase is identified as pitting potential E_{pit}, and the potential at which the reverse scan intersects the forward one is regarded as the repassivation/protection potential Eprot. For 5A02 aluminum alloy, the onset of pitting is not visible since the pitting potential E_{pit} coincides with the corrosion potential E_{corr}, due to the O_2-enhanced pitting corrosion[30]. As reported by Shibata and other researchers[31-33], E_{pit} is a distributed parameter and the probability of E_{pit} can be determined as: $P(E_{pit} < E(n)) = n/(N+1)$, where N is the total number of samples studied

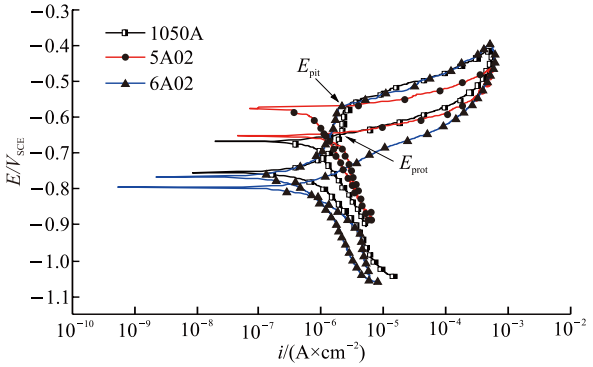

Fig.7 Cyclic polarization (CP) curves of pure Al 1050A, 5A02 and 6A02 aluminum alloys in aerated 0.1M NaCl solution

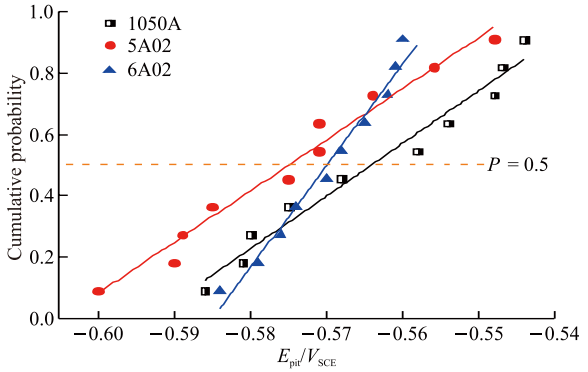

Fig.8 The distributions of pitting potential of pure Al 1050A, 5A02 and 6A02 aluminum alloys

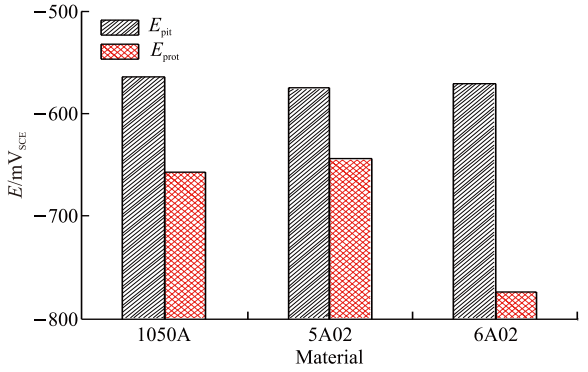

Fig.9 Comparison of the pitting potential (E_{pit}) and protection potential (E_{prot}) of the three metals

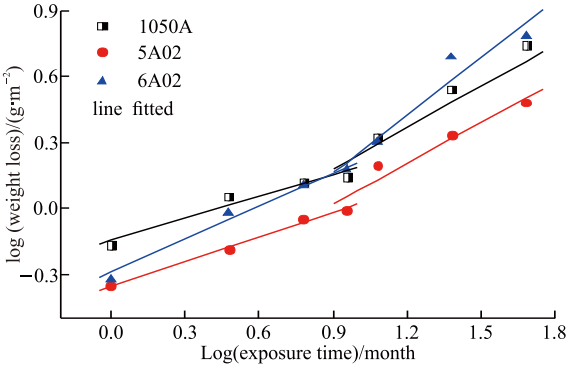

Fig.10 Bilogarithmic plots of data points from Fig.2(a) and the corresponding fitting results

and n is the number of samples pitted at a potential E or lower[32]. The potential at $P = 0.5$ is a representative value of E_{pit} for a given alloy. In this work, the same method is utilized and the corresponding cumulative distribution plot of E_{pit} is shown in Fig.8. The distribution shown in Fig.8 is consistent with what has been observed in Al systems[14,32] and supports the view that E_{pit} is a distributed parameter. The protection potential E_{prot} is also calculated using the same method and depicted in Fig.9 accompanied by E_{pit}. It can be seen that the E_{pit} decreases (shift negatively) successively in the order: 1050A > 6A02 > 5A02, while the E_{prot} decreases following the sequence: 5A02 > 1050A > 6A02.

4 Discussion

4.1 Corrosion kinetics of aluminum and its alloys in tropical marine atmosphere

In general, corrosion weight loss of metals exposed to the atmospheric environment follows the well-known bilogarithmic equations:

$$C=At^n \tag{3}$$

where C is the weight loss (g/m^2), t is the exposure time (month) and A and n are constants. Townsend and Zoccola[34] have proposed a method to analyze corrosion data using linear regression analysis to fit a straight line on log–log plot by taking the logarithm of Eq. (3):

$$\log C=\log A+n\log t \tag{4}$$

Fig.10 reproduces the results in Fig.2(a) by plotting the weight loss against the exposure time in log-log coordinates. It is obvious that the curves can be well fitted by two distinct lines, which take the ninth month as the turning point. This phenomenon was also observed on pure Al 1060 in our previous work[35]. The fitting results of the two linear segments are shown in Table 3, in which R represents the correlation coefficients. The slope of the fitting lines, n, is a significant parameter that can be considered as an indicator for the physicochemical behavior of the corrosion product layer and hence for its interactions with the atmospheric environment[36]. It is found that the slopes of the second segment are higher than 0.5 while that of the first segment are lower than 0.5 for all the three metals. The n values depend on the metal concerned, the local atmosphere and the exposure conditions[36]. Here in this work, the higher n values of the second segment after exposure for 9 months are mainly attributed to the environmental variation especially the Cl^- deposition rate and the TOW. As shown in Fig.1, after exposure for 9 months, the Cl^- deposition rate improves noticeably and the TOW keeps a relatively higher value. Consequently, the metal surface is easy to form adsorbed thin electrolyte layer due to the formation of corrosion products and deposition of salt particles, which results in the acceleration of weight loss[23]. The fast increase of corrosion coverage area during this period (Fig.3) can also be explained by this inference. The existence of Cl^- and electrolyte layer provides more chances to nucleate pits and thus leads to a higher corrosion area. It is worth to note that the n value of the second segment for 6A02 alloy is higher than the other ones, indicating that the 6A02 alloy is the most sensitive to Cl^-[37].

4.2 Comparison of the corrosion behavior between the pure aluminum and its alloys

In tropical marine atmosphere, the synergetic effect of high Cl^- deposition rate and high relative humidity provides favorable conditions for serious pitting corrosion. For aluminum alloys, the electrochemical approach describes pitting corrosion in terms of nucleation events, metastable pitting and stable pitting[32, 38, 39]. In Figs.4-6, many metastable pits are observed in the initial exposure period. This is mainly attributed to the inhibition of wet-dry cycles to the stable pits formation. Certainly, some of them can grow continuously to form stable pits. Here in this work, all the three metals experience pitting corrosion during the exposure tests. But there exist some differences among them. Firstly, the alloy 5A02 has the lowest weight loss and the largest corrosion coverage, indicating that

Table 3 Fitting results of the lines in Fig.10

Item	First stage		Second stage	
	$\log C=\log A+n\log t$	R^2	$\log C=\log A+n\log t$	R^2
1050A	$\log C=-0.142\ 7+0.329\ 9t$	0.973	$\log C=-0.571\ 4+0.792\ 9t$	0.980
5A02	$\log C=-0.353\ 1+0.372\ 2t$	0.997	$\log C=-0.538\ 0+0.619\ 9t$	0.936
6A02	$\log C=-0.319\ 3+0.532\ 6t$	0.999	$\log C=-0.614\ 0+0.874\ 0t$	0.937

the alloy is the most sensitive to pitting initiation but insensitive to growth in depth. As shown in Fig.5, the pits incline to spread laterally to connect with each other, resulting in the flaking of the surface layer on the specimen. On the contrary, the alloy 6A02 presents the highest weight loss but the lowest corrosion coverage, meaning that the pitting nucleation rate is low but the pitting propagation rate is high. Once a pit generates on 6A02 alloy, it tends to grow in depth and form a deep hole (Fig.6). The differences in corrosion of the three metals can be further confirmed by the CP results in Fig.7. For 5A02 aluminum alloy, the onset of pitting is not visible due to the O_2-enhanced pitting corrosion, and the anodic Tafel slope is practically zero[30, 40]. In this case, the initiation of pitting corrosion is easy to occur under the natural state, which results in the higher corrosion coverage (Fig.3) and shallower corrosion pits (Fig.5). In comparison, the 6A02 aluminum alloy presents the most positive E_{pit} value which verifies the difficulty of pit initiation and the most negative E_{prot} value which implies the poor repassivation kinetics of this alloy[40]. Therefore, pits in 6A02 alloy incline to grow in depth.

5 Conclusions

Atmospheric corrosion behavior of pure Al 1050A, 5A02 and 6A02 aluminum alloys in a tropical marine atmosphere was investigated in this work. Influences of environmental conditions on the corrosion kinetics and the pitting corrosion resistance of the three metals were discussed. The main conclusions were made as follows:

a) Weight loss of the three metals can be well fitted with two linear segments in the log-log coordinates, which is attributed to the variation of Cl^- deposition rate and TOW.

b) Weight loss of the three metals decreases in the order: 6A02 > 1050A > 5A02, while the corrosion coverage area presents the opposite tendency.

c) Pits on 5A02 alloy are easy to initiate and incline to spread laterally to form higher corrosion area and shallower corrosion pits.

d) Pits on 6A02 alloy are difficult to initiate but easy to propagate in depth to generate lower corrosion area and deeper corrosion pits.

References

[1] Romhanji E, Popović M. Problems and Prospect of Al-Mg Alloys Application in Marine Constructions[J]. *Metalurgija*, 2006, 12(4): 297-307

[2] Kwon K, Frangopol D M. Fatigue Life Assessment and Lifetime Management of Aluminum Ships Using Life-cycle Optimization[J]. *J. Ship Res*., 2012, 56(2): 91-105

[3] Sielski R A. Research Needs in Aluminum Structure[J]. *Ships Offshore Struc*., 2008(1), 3: 57-65

[4] Szklarska-Smialowska Z. Pitting Corrosion of Aluminum[J]. *Corros. Sci*., 1999, 41(9): 1 743-1 767

[5] McCafferty E. Sequence of Steps in the Pitting of Aluminum by Chloride Ions[J]. *Corros. Sci*., 2003, 45(7): 1 421-1 438

[6] Frankel G S. Pitting Corrosion of Metals a Review of the Critical Factors[J]. *J. Electrochem. Soc*., 1998, 145(6): 2 186-2 198

[7] Boag A, Taylor R, Muster T, *et al.* Stable Pit Formation on AA2024-T3 in a NaCl Environment[J]. *Corros. Sci.*, 2010, 52(1): 90-103

[8] Boag A, Hughes A, Glenn A, *et al*. Corrosion of AA2024-T3 Part I: Localised Corrosion of Isolated IM Particles[J]. *Corros. Sci.*, 2011, 53(1): 17-26

[9] Aballe A, Bethencourt M, Botana F, *et al.* Localized Alkaline Corrosion of Alloy AA5083 in Neutral 3.5% NaCl Solution[J]. *Corros. Sci.*, 2001, 43(9): 1 657-1 674

[10] Eckermann F, Suter T, Uggowitzer PJ, *et al*. The Influence of MgSi Particle Reactivity and Dissolution Processes on Corrosion in Al-Mg-Si Alloys[J]. *Electrochim. Acta*, 2008, 54(2): 844-855

[11] Yasakau K A, Zheludkevich M L, Lamaka S V, *et al*. Role of Intermetallic Phases in Localized Corrosion of AA5083[J]. *Electrochim. Acta*, 2007, 52(27): 7 651-7 659

[12] De la Fuente D, Otero-Huerta E, Morcillo M. Studies of Long-term Weathering of Aluminium in the Atmosphere[J]. *Corros. Sci.*, 2007, 49(7): 3 134-3 148

[13] Liu Y, Wang Z, Ke W. Study on Influence of Native Oxide and Corrosion Products on Atmospheric Corrosion of Pure Al[J]. *Corros. Sci*., 2014, 80: 169-176

[14] Kim Y, Buchheit R G. A Characterization of the Inhibiting Effect of Cu on Metastable Pitting in Dilute Al-Cu Solid Solution Alloys[J]. *Electrochim. Acta*, 2007, 52(7): 2 437-2 446

[15] Mukhopadhyay A. Selection and Design Principles of Wrought Aluminium Alloys for Structural Applications[J]. *Mater. Sci. Forum*, 2012, 710: 50-65

[16] Cui Z Y, Li X G, Xiao K, *et al*. Corrosion Behavior of Field-exposed Zinc in a Tropical Marine Atmosphere[J]. *Corrosion*, 2014, 70(7): 731-748

[17] International Organization for Standardization. *Corrosion of Metals and Alloys-Classification of Corrosivity of Atmospheres*[S]. ISO 9223,1992

[18] Schindelholz E, Kelly R, Cole I S, *et al*. Comparability and Accuracy of Time of Wetness Sensing Methods Relevant for Atmospheric Corrosion[J]. *Corros. Sci.*, 2013, 67: 233-241

[19] Cole I S, Ganther W, Sinclair J, *et al*. A Study of the Wetting of Metal Surfaces in Order to Understand the Processes Controlling Atmospheric Corrosion[J]. *J. Electrochem. Soc*., 2004, 151(12): B627-B635

[20] Cole I S, Ganther W. Experimental Determination of Duration of Wetness on Metal Surfaces[J]. *Corros. Eng. Sci. Technol.*, 2008, 43(2): 156-162

[21] Corvo F, Pérez T, Martin Y, *et al*. Time of Wetness in Tropical Climate: Considerations on the Estimation of TOW According to ISO 9223 Standard[J]. *Corros. Sci.*, 2008, 50(1): 206-219

[22] International Organization for Standardization. *Corrosion of Metals and Alloys-Corrosivity of Atmospheres-Measurement of Pollution*[S]. ISO 9225, 1992

[23] Cui Z Y, Li X G, Xiao K, *et al*. Atmospheric Corrosion of Field-exposed AZ31 Magnesium in a Tropical Marine Environment[J]. *Corros. Sci*., 2013, 76: 243-256

[24] Ma Y, Li Y, Wang F. The Effect of β-FeOOH on the Corrosion Behavior of Low Carbon Steel Exposed in Tropic Marine Environment[J]. *Mater. Chem. Phy.*, 2008, 112(3): 844-852

[25] Ma Y, Li Y, Wang F. The Atmospheric Corrosion Kinetics of Low Carbon Steel in a Tropical Marine Environment[J]. *Corros. Sci*., 2010, 52(5): 1 796-1 800

[26] Ma Y, Li Y, Wang F. Corrosion of Low Carbon Steel in Atmospheric Environments of Different Chloride Content[J]. *Corros. Sci*., 2009, 51(5): 997-1 006

[27] Sun S, Zheng Q, Li D, *et al*. Long-term Atmospheric Corrosion Behaviour of Aluminium Alloys 2024 and 7075 in Urban, Coastal and Industrial Environments[J]. *Corros. Sci*., 2009, 51(4): 719-727

[28] Dan Z, Muto I, Hara N. Effects of Environmental Factors on Atmospheric Corrosion of Aluminium and Its Alloys Under Constant Dew Point Conditions[J]. *Corros. Sci*., 2012, 57: 22-29

[29] Graedel T E. Corrosion Mechanisms for Aluminum Exposed to the Atmosphere[J]. *J. Electrochem. Soc.*, 1989, 136(4): 204C-212C

[30] Trueba M, Trasatti S P. Study of Al Alloy Corrosion in Neutral NaCl by the Pitting Scan Technique[J]. *Mater. Chem. Phy*., 2010, 121(3): 523-533

[31] Shibata T, Takeyama T. Stochastic Theory of Pitting Corrosion[J]. *Corrosion*, 1977, 33(7): 243-251

[32] Gupta R, Sukiman N, Cavanaugh M, *et al*. Metastable Pitting Characteristics of Aluminium Alloys Measured Using Current Transients During Potentiostatic Polarisation[J]. *Electrochim. Acta*, 2012, 66: 245-254

[33] Zhang T, Yang Y, Shao Y, *et al.* A Stochastic Analysis of the Effect of Hydrostatic Pressure on the Pit Corrosion of Fe-20Cr Alloy[J]. *Electrochim. Acta*, 2009, 54(15): 3 915-3 922

[34] Townsend H E, Zoccola J C. *STP767*[M]. Philadelphia: ASTM, 1982

[35] Cui Z Y, Li X G, Xiao K, *et al.* Atmospheric Corrosion Behaviour of Pure Al 1060 in Tropical Marine Environment[J]. *Corros. Eng. Sci. Technol.*, 2015, 50(6): 438-448

[36] De la Fuente D, Díaz I, Simancas J, *et al*. Long-term Atmospheric Corrosion of Mild Steel[J]. *Corros. Sci*., 2011, 53(2): 604-617

[37] Cao C N. *Material Natural Environmental Corrosion of China*[M]. Beijing: Chemistry Industry Press, 2005

[38] Amin M A. Metastable and Stable Pitting Events on Al Induced by Chlorate and Perchlorate Anions-Polarization, XPS and SEM Studies[J]. *Electrochim. Acta*, 2009, 54(6): 1 857-1 863

[39] Trueman A R. Determining the Probability of Stable Pit Initiation on Aluminium Alloys Using Potentiostatic Electrochemical Measurements[J]. *Corros. Sci.*, 2005, 47(9): 2 240-2 256

[40] Zaid B, Saidi D, Benzaid A, *et al.* Effects of pH and Chloride Concentration on Pitting Corrosion of AA6061 Aluminum Alloy[J]. *Corros. Sci*., 2008, 50(7): 1 841-1 847